Article

Fabrication and In Vitro Characterization of Novel Hydroxyapatite Scaffolds 3D Printed Using Polyvinyl Alcohol as A Thermoplastic Binder

Andrej Thurzo [1,*], Paulína Gálfiová [2], Zuzana Varchulová Nováková [3,4], Štefan Polák [2], Ivan Varga [2], Martin Strunga [1], Renáta Urban [1], Jana Surovková [1], Ľuboš Leško [3] Zora Hajdúchová [5], Jozef Feranc [6], Marian Janek [5,7], Ľuboš Danišovič [3, 4, *]

[1] Department of Orthodontics, Faculty of Medicine, Comenius University in Bratislava, 81250 Bratislava, Slovakia; Thurzo3@uniba.sk; strunga2@uniba.sk; urban96@uniba.sk; surovkova6@uniba.sk;
[2] Institute of Histology and Embryology, Faculty of Medicine, Comenius University, Sasinkova 4, 81104 Bratislava, Slovakia ; galfiova1@uniba.sk; stefan.polak@fmed.uniba.sk; ivan.varga@fmed.uniba.sk;
[3] Institute of Medical biology, Genetics and Clinical Genetic, Faculty of Medicine, Comenius University, Sasinkova 4, 811 08 Bratislava, Slovakia; varchulova2@uniba.sk; lesko13@uniba.sk, lubos.danisovic@fmed.uniba.sk;
[4] National Institute of Rheumatic Diseases, Nábrežie I. Krasku 4, 921 12 Piešťany, Slovakia;
[5] Slovak University of Technology, Faculty of Chemical and Food Technology, Department of Inorganic Materials, Radlinského 9, 81237 Bratislava, Slovakia; marian.janek@stuba.sk;
[6] Slovak University of Technology, Faculty of Chemical and Food Technology, Department of Plastics, Rubber and Fibres, Radlinského 9, 81237 Bratislava, Slovakia; jozef.feranc@stuba.sk;
[7] Comenius University, Faculty of Natural Sciences, Department of Physical and Theoretical Chemistry, Mlynská dolina, Ilkovičova 6, CH1, 84215 Bratislava, Slovakia; marian.janek@uniba.sk;
* Correspondence: Thurzo3@uniba.sk (A.T.), lubos.danisovic@fmed.uniba.sk (Ľ.D.)

Abstract: This paper presents a proof-of-concept study on the biocolonization of 3D-printed hydroxyapatite scaffolds with mesenchymal stem cells (MSCs). Three-dimensional (3D) printed biomimetic bone structure made of Calcium Deficient HydroxyApatite (CDHA) intended as future bone graft was made from newly developed composite material for FDM printing. The biopolymer polyvinyl alcohol serves in this material as a thermoplastic binder for 3D molding of the printed object with a passive function and is completely removed during sintering. The study presents the material, the process of fused deposition modeling (FDM) of CDHA scaffolds and its post-processing at three temperatures (1200, 1300, 1400 °C), as well it evaluates the cytotoxicity and biocompatibility of scaffolds with MTT and LDH release assays after 14 days. The study also includes a morphological evaluation of the cellular colonization with scanning electron microscopy (SEM) in two different filament orientations (rectilinear and gyroid). The results of the MTT assay showed that the tested material was not toxic, and cells were preserved in both orientations, with most cells present on the material fired at 1300°C. Results of the LDH release assay showed a slight increase in LDH leakage from all samples. Visual evaluation of SEM confirmed the ideal post-processing temperature of the 3D-printed FDM framework for samples fired at 1300°C and 1400°C, with a porosity of 0.3 mm between filaments. In conclusion, the presented fabrication and colonization of CDHA scaffolds have great potential to be used in the tissue engineering of bones.

Keywords: Regenerative dentistry; 3D printing; biomimetic; bioinspired materials; MSC; cell colonization; Tissue engineering; Regenerative medicine; Oral Bone; Tissue Regeneration; biocolonization; CDHA, MTT; LDH; SEM; FDM.

1. Introduction

Hydroxyapatite (HA) has been used in regenerative medicine as an inert scaffold since the 1950s. Due to its high osteoconductivity and biocompatibility, it is widely used in bone tissue engineering [1,2]. Regenerative dentistry plays a promising role in all areas

 doi:10.20944/preprints202211.0141.v1

of dentistry, especially in periodontology and implantology in the treatment of bone defects in teeth and implants [3].

Various craniofacial and dental surgical procedures require reconstruction of bone defects caused by trauma, disease, tumor resection, or simply premature tooth loss. The dental arch after tooth extraction begins to lose bone in the corresponding part of the alveolar bone [4,5]. This effect may prevent the usual therapeutic scenario of dental implant placement due to the lack of supporting bone for the planned dental implant.

Globally, millions of bone graft procedures are being performed by clinicians annually to treat the rising prevalence of bone defects. **Calcium-phosphate-based** biomaterials have excellent properties and are widely used to repair bone defects due to their similarity to the inorganic components of human bone. Hydroxyapatite (HA) as the thermodynamically most stable crystalline phase of CaP in aqueous solutions is mostly used in the form of ceramics or composite frameworks with polymers [6]. It is considered as a promising scaffold material also for dental and orthopedic implants due to its ideal biocompatibility and high osteoconductivity. The implants morphology modification has been extensively studied to regulate the host immune environment and further promote bone regeneration [7,8].

Current advances in **HA-based bio composites** for bone tissue regeneration in regenerative dentistry are opening new therapeutical opportunities. Bone tissue is a nanocomposite constituted of an organic and inorganic matrix in which the collagen component and the mineral phase are organized in complex and porous structures. HA is therefore the most used ceramic biomaterial, as it mimics the mineral composition of human bone. However, this biomimetic material has poor mechanical properties, such as low tensile and compressive strength, making it less than ideal for bone tissue engineering. HA bio composites are generally biocompatible, as demonstrated by most in vitro and in vivo studies in animal models [9].

The repair of critical size in alveolar bone defects is still an unmet clinical need, and in recent decades materials scientists have made efforts to find effective technological solutions based on the use of suitable scaffolds. Although calcium phosphates are widely accepted as biomaterials for the fabrication of regenerative bone scaffolds, their processing into 3D devices with suitable cell-instructive properties is still hindered by insurmountable drawbacks [10]. Successful bone reconstruction requires the development and use of bone grafts that have structural, functional, and biological properties like those of natural tissue [11,12]. Research in this paper reports feasibility of prospective clinical scenarios for bone augmentations personalized in 3D shape and on cellular level. Such homologous bone scaffolds, individualized in shape and colonized with the patient's own cells, are a tantalizing scenario for which effective and safe manufacturing still needs to be found. An approximation of the possible scenario is shown in Figure 1. As exemplified in **Figure 1a**, extraction of the mandibular first molar may result in extensive loss of alveolar bone, followed by smoothing of the natural bone ridges and remodeling, typically leading to further recession of the alveolar bone level in this area (**Figure 1b**). Cone beam computed tomography (CBCT) segmentation and matching of the two models can reveal the extent of bone remodeling (**Figure 1c**). **Figure 1d** shows a prospective scenario for the use of colonized scaffolds in clinical situations where augmentation of the alveolar bone is required. The advantage of such an application is the ideal complementarity of the 3D shape and the biological compatibility.

Preprints (www.preprints.org) | NOT PEER-REVIEWED | Posted: 8 November 2022 doi:10.20944/preprints202211.0141.v1

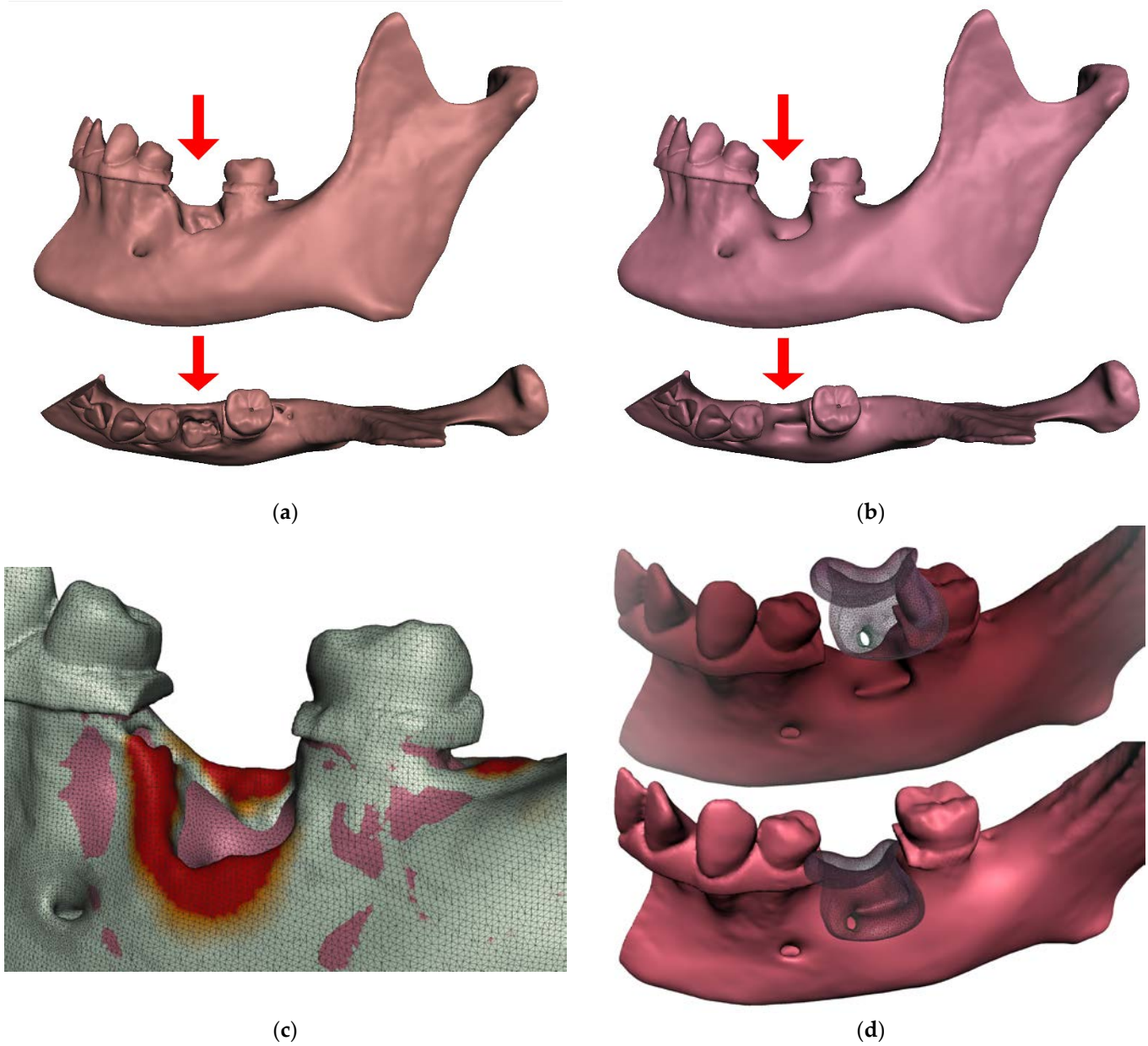

Figure 1. Following tooth extraction, the alveolar ridge undergoes an inevitable remodeling process. The concept of prospective clinical application of colonized 3D printed personalized scaffolds: (**a**) Extraction of a molar in the mandible can be the cause of an extensive loss of alveolar bone; (**b**) Smoothing of the natural bone ridges and remodeling, typically leading to further recession of the alveolar bone level in this area; (**c**) A differential heat map of the comparison of aligned segmented CBCT models may reveal the extent of bone remodeling that has occurred; (**d**) A prospective scenario for the use of colonized scaffolds in clinical situations where augmentation of alveolar bone is required.

Three-dimensional (3D) printing is a promising technology for a variety of healthcare applications, from regenerative medicine and tissue engineering to production of clinical appliances [13–17]. From comparison of conventional biofabrication methods with 3D printing, it is evident that the potential of 3D printing to produce on-demand, personalized, and complex products is unparalleled. Recent trends in the use of 4D materials (printed materials that change over time or in response to stimuli) can be used to overcome many of the inherent limitations of traditional 3D printing technologies [18].

Although the clinical application of bone printing technology is still in its infancy, the production of whole and functional bone parts characterized by an appropriate shape

 doi:10.20944/preprints202211.0141.v1

is an attractive and significant challenge in tissue engineering. Bone printing, such as cell source selection and achieving viable vascularization within the newly printed bone, is a major challenge in efforts to create 3D dense tissue, as this requires the development of an appropriate vascular supply. Biologically printed bone has been successfully implanted in preclinical models, and 3D-printed plastic, ceramic, or metal implants for bone tissue replacement [19] have been successfully transplanted into humans [20,21].

More than a decade ago, advances in polymer manufacturing enabled the development of hybrid systems consisting of multiple polymer formulations in different physical configurations. In 2009, Quigley et al. presented a hybrid polymer platform consisting of biodegradable polymer fibers. Taking advantage of the properties of conductive and biodegradable polymers, their scaffold was designed to promote directional axonal growth and migration of Schwann cells via the microstructure of the biodegradable polymer fibers [22]. Also, a recent study of Wiatrak et al. 2021, showed that nanocrystalline apatite doped and co-doped with Li^{+} and Eu^{3+} ions may be a very attractive biomaterial for the regeneration of nervous tissue, where europium ions influence neuronal features even more strongly than doping with lithium alone [23].

The biopolymer presented in this study is polyvinyl alcohol (PVA), which is only used as a passive thermoplastic binder for 3D molding during 3D objects printing. It is a water-soluble synthetic polymer that, when heated to temperatures above 250 degrees in the air, the thermal degradation oxidation processes are present, resulting in formation of water and carbon dioxide as main products. Some of the most common medical applications of PVA are soft contact lenses, eye drops, embolization particles, tissue adhesion barriers, artificial cartilage, and meniscus. PVA has been explored in the production of fibers that align and promote proliferation and cell-cell interactions of renal cells [24] or has been explored in its oxidized form as a new polymer to produce nerve conduits [25]. PVA-based composite hydrogels are also promising materials with various biomedical applications. However, their mechanical and tribological properties often need to be modified. For example, the study of Feng et al. 2022 on the preparation of PVA gellan gum hydrogels showed the effects on their rheological and tribological properties [26].

The application of biomimetic strategies and bioinspired materials is widely used in the field of regenerative dentistry [27]. 3D printing of bone scaffolds can be performed using various 3D printing techniques such as FDM, powder sintering and many others [20]. This is also true for pore geometry, which has a great influence on the cellular response. This is why 3D printing is such an attractive technology for bone tissue engineering, as it allows complete control and shaping of porosity. Calcium phosphate materials synthesized from natural sources have recently attracted some interest because they closely resemble natural bone and have better bioactivity than synthetic compounds [28].

Only recently has been published research highlighting importance of surface properties. The study by Devi et al. 2022 designed a fucoidan from Sargassum ilicifolium incorporated in an osteo-inductive scaffold comprising calcium crosslinked sodium alginate-nano hydroxyapatite-nano graphene oxide (Alg-HA-GO-F), which tends to serve as a bone graft substitute. The SEM revealed highly suitable surface properties, such as porosity and nanoscale roughness. The physical, structural, and enriching osteogenic potential results of Alg-HA-GO-F indicate that it can be a potential bone graft substitute for orthopedic applications [29]

The internal geometry of the scaffolds is only one aspect. In regenerative dentistry, the key aspect related to advanced dental implants, bone and soft tissue regeneration using autologous grafts or xenografts, allografts, their integration, and acceptance does not depend only on the material. The host response also plays a very important role through its vascularization [30].

 doi:10.20944/preprints202211.0141.v1

As it was highlighted, the chemical composition and surface topology of tissue-engineered scaffolds are two crucial parameters for regulating cell behavior [31], albeit processes following the colonization of the scaffold are also relevant to the cell differentiation aspect. For example, mechanical stimuli play a role in osteogenesis and chondrogenesis [32].

The use of mesenchymal stem cells (MSCs) in regenerative therapeutic procedures is becoming an increasingly important topic in medicine. Since the first isolation of MSCs derived from dental tissue, the properties and potential of these cells in regenerative dentistry have been intensively studied. Their multidifferentiation potential, self-renewal ability, and ease of access give them a key role in stem cell-based therapy. To date, several types of dental stem cells have been discovered, and their potential use can be found in most of the major branches of dentistry. Dental tissue-derived MSCs have been shown to be a valuable stem cell source with great therapeutic potential. Despite a respectable number of in vitro and in vivo studies on MSCs treatment in regenerative dentistry, there are still factors that need to be overcome in order to establish more predictable and reliable clinical protocols [33]. Dental stem cells are often used for oral regenerative applications [34]. Gingival stem cells are a limitless reservoir for regenerative medicine. Gingival tissue can be easily collected and represents an accessible source for the isolation of gingival mesenchymal stem cells (GMSCs). GMSCs are a subpopulation of gingival-derived mesenchymal stem cells that exhibit the characteristics of mesenchymal stem cells (MSCs), such as differentiation capacity and immunomodulatory properties. Dental stem cells are also expandable in vitro, genomically stable, and have the ability to maintain their stem cell properties over time. GMSCs should be considered as a good stem cell source for potential applications in tissue engineering and regenerative dentistry [35].

3D bioprinting in dentistry is unfortunately not yet close to clinical reality. Therefore, further research on the fabrication of ideal bioinks with implantation into larger animal models in the oral environment is urgently needed for clinical implementation [36].

The current clinical reality is well reviewed in the recent study focused on available in vivo studies of oral bone tissue regeneration using MSCs. In general, unseeded scaffolds have shown limited regenerative potential. The bone regenerative potential of scaffolds enriched with MSCs can be influenced and improved by the addition of biomolecules, such as bone morphogenetic proteins, or the modulation of biomaterial features, such as pore dimension. Most of the studies used composite scaffolds or biomaterials with surface modifications, together with MSCs [37].

The aim of this paper is to introduce a composite filament based on hydroxyapatite material suitable for FDM 3D printing for novel scaffolds fabrication with perspective of full cellular and 3D shape personalization. Paper also presents in vitro characterization of this material after colonization with MSCs.

2. Results

The scaffolds were printed in rectilinear / gyroid layer arrangement and three sintering temperatures 1200°C, 1300°C and 1400°C were used. The cells adhered well to both layer arrangements and were comparable to the control group. Most of cells were observed on material fired at 1300°C and 1400°C, the fewest at the lowest temperature. None of the samples showed an increased rate of leaching of LDH into solution. Scaffold material prepared at 1200°C had a slight inhibitory effect on cell proliferation.

MTT assay

Preprints (www.preprints.org) | NOT PEER-REVIEWED | Posted: 8 November 2022 doi:10.20944/preprints202211.0141.v1

To evaluate the potential of fabricated materials, cytotoxicity study was conducted by MTT assay as a first step. The results of MTT assay presented in **Figure 2** showed that all analyzed materials were non-toxic and structure of the scaffold did not have a significant impact on the proliferation of MSCs. When compared with negative control, the best results were obtained in the case of material processed at 1300°C and 1400°C. However, the material prepared at 1200°C had inhibitory effect on cell proliferation.

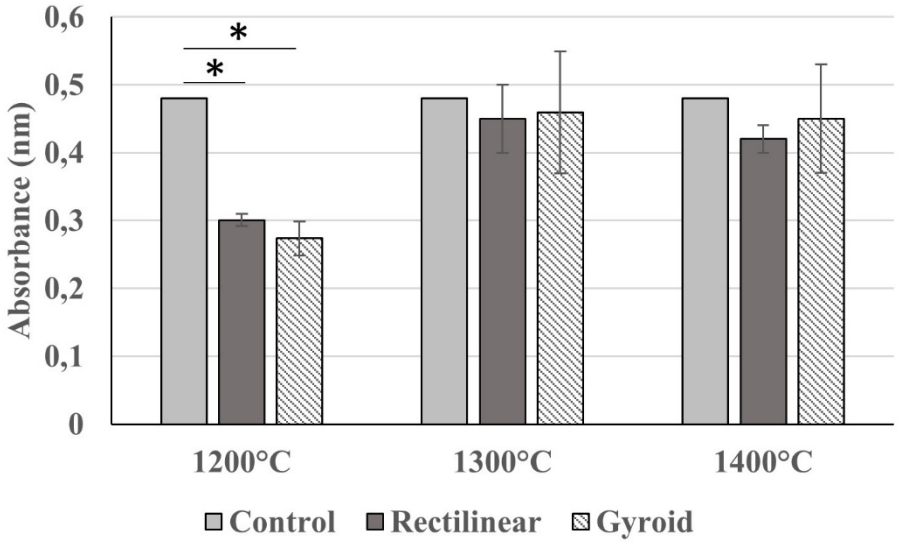

Figure 2. Results of MTT assay. Results of MTT assay. Analysed scaffolds processed at 1300°C and 1400°C were non-toxic. Only in the case of scaffolds processed at 1200°C we recorded a significant inhibitory effect when compared with the control.

LDH Release Assay

LDH release assay was used to estimate material cytotoxicity by releasing LDH as a substitute marker for membrane disruption in human cells. The results of LDH release assay presented in **Figure 3** demonstrated that all analyzed materials showed a slight increase in LDH leakage of ASCs into the culture medium.

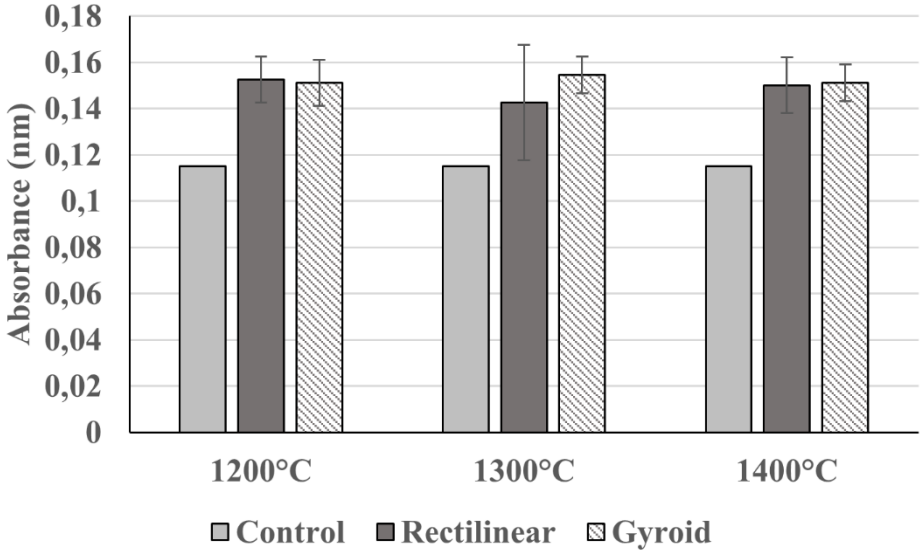

Figure 3. Results of LDH release assay. LDH accumulation changes in the case of all analysed scaffolds were insignificant, suggesting good biocompatibility.

 doi:10.20944/preprints202211.0141.v1

Characteristics of used material

The morphology of Calcium Deficient HydroxyApatite (CDHA) particles observed under SEM revealed almost spherical aggregates (**Figure 4a**) that were composed of primary HA crystals around 100 nm in size, when the top surface of aggregate was observed (**Figure 4b**). Perpendicular filament fracture areas made under cryogenic conditions showed homogeneous surface characteristics with well distributed CDHA in used polymeric binder (**Figure 4c**). Indeed, magnified fracture surface (15 000 ×) **Figure 4d** shows, that good distribution of primary HA crystals was achieved from CDHA aggregates during filament preparation, while cryogenic filament fracturing also generated some fissures longer than 1 μm (**Figure 4d**).

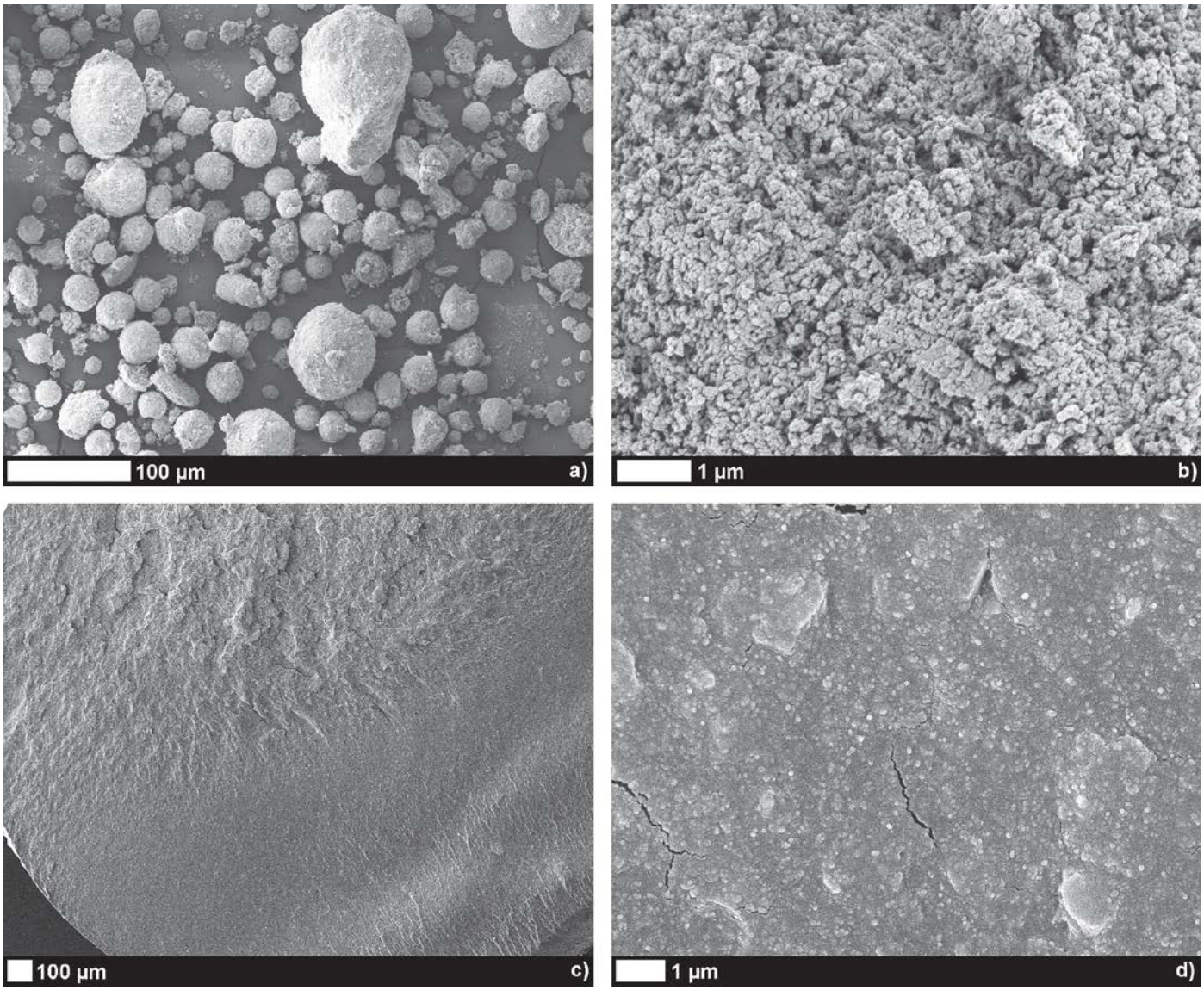

Figure 4. SEM images of: (**a**) spherical aggregates of used CDHA; (**b**) enlarged surface image of the CDHA aggregate; (**c**) filament fracture surface; (**d**) enlarged fracture surface image with several fissures produced during filament fracturing under cryogenic conditions.

For biomedical applications, the comprehensive characteristics of investigated CDHA powder are important indicators of specific physical-chemical characteristics of the materials used. The XRPD pattern of CDHA revealed relatively broad diffraction peaks for low crystalline HA structure with corresponding (hkl) indexes (**Figure 5**). The

 doi:10.20944/preprints202211.0141.v1

evaluation in Match!© software (Crystal Impact GbR, Bonn, Germany), confirmed the hydroxyapatite structure according to the Crystallography Open Database entrance 96-900-1234 (COD-Inorg 2021.06.14). The effect of heating on CDHA crystal structure is reflected by XRPD pattern shown in **Figure 5** and selected temperature 1300 °C. The heating induced the narrowing of diffraction peaks, indicating improvement of HA crystallinity. At the same time, two diffractions of lesser intensity are observed at 36.4 and 40.3 °2Θ (denoted by stars in **Figure 5**). These two diffractions correspond to the new phase developed by heating and correspond to the most intense diffraction peaks of β-TCP produced by dehydroxylation reaction of HA [38]. Hence, the sintering of CDHA to desired temperature 1300 °C forms biphasic calcium phosphate biomaterial with changed bioactivity [39].

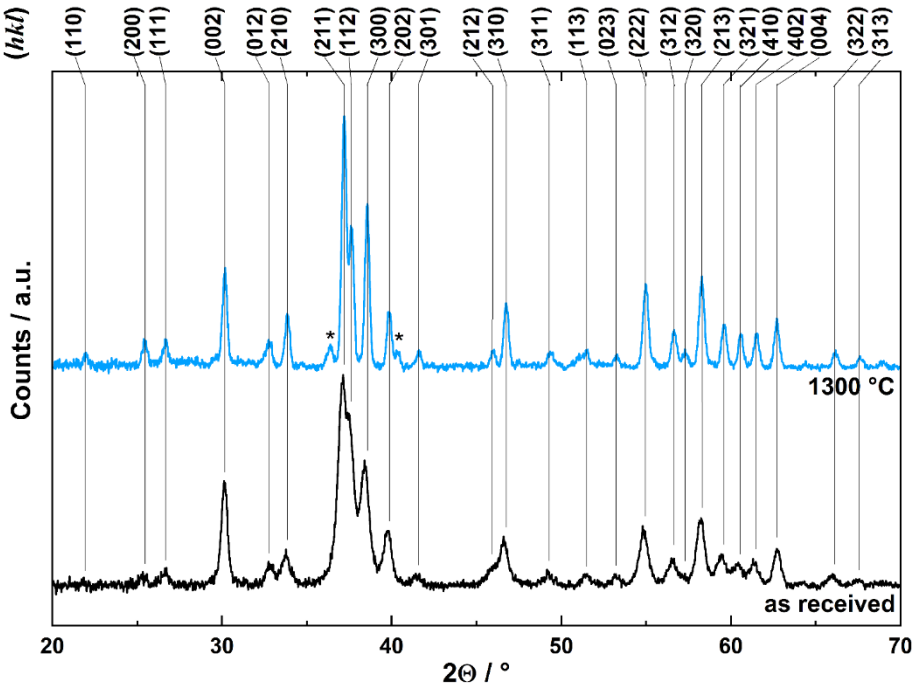

Figure 5. X-ray diffraction patterns of as received CDHA (bottom) and after the material sintering at 1300 °C (top) with respective (hkl) indexes.

The characteristics of CDHA were also investigated by ATR-FTIR spectroscopy. The spectrum of original CDHA as received from the supplier is shown in the **Figure 6**, bands identification was proved by structure isotopic substitution by Fowler 1974 [40]. as follows: band observed at 3571 cm^{-1} correspond to the OH stretching mode, while the librational mode of OH groups is observed at 630 cm^{-1}; the bands observed at 1090 cm^{-1} and 1028 cm^{-1} including shoulder around 1063 cm^{-1} correspond to triply degenerated ν_3 antisymmetric PO_4^{3-} stretching mode, the band observed at 962 cm^{-1} represent ν_1 nondegenerate PO_4^{3-} symmetric stretching vibration, the band at 601 cm^{-1} is the component of triply degenerate ν_4 O–P–O bending mode vibration. The lower frequency bending modes are not shown due to the absorption edge of ZnSe crystal used in ATR module. After CDHA sintering at 1300 °C the band intensities corresponding to stretching and librational modes of structural OH groups strongly decreased as expected due to the structural dehydroxylation of CDHA (**Figure 6**). The band intensities of PO_4^{3-} anions also decreased and the triply degenerated ν_3 antisymmetric PO_4^{3-} stretching bands are resolved and detected at 1090 cm–1, 1047 cm^{-1} and 1024 cm^{-1}, new developed side bands at 997 and 943 cm^{-1} of the band observed at 962 cm^{-1} may represent ν_1 degenerate PO_4^{3-} symmetric stretching vibrations.

Preprints (www.preprints.org) | NOT PEER-REVIEWED | Posted: 8 November 2022 doi:10.20944/preprints202211.0141.v1

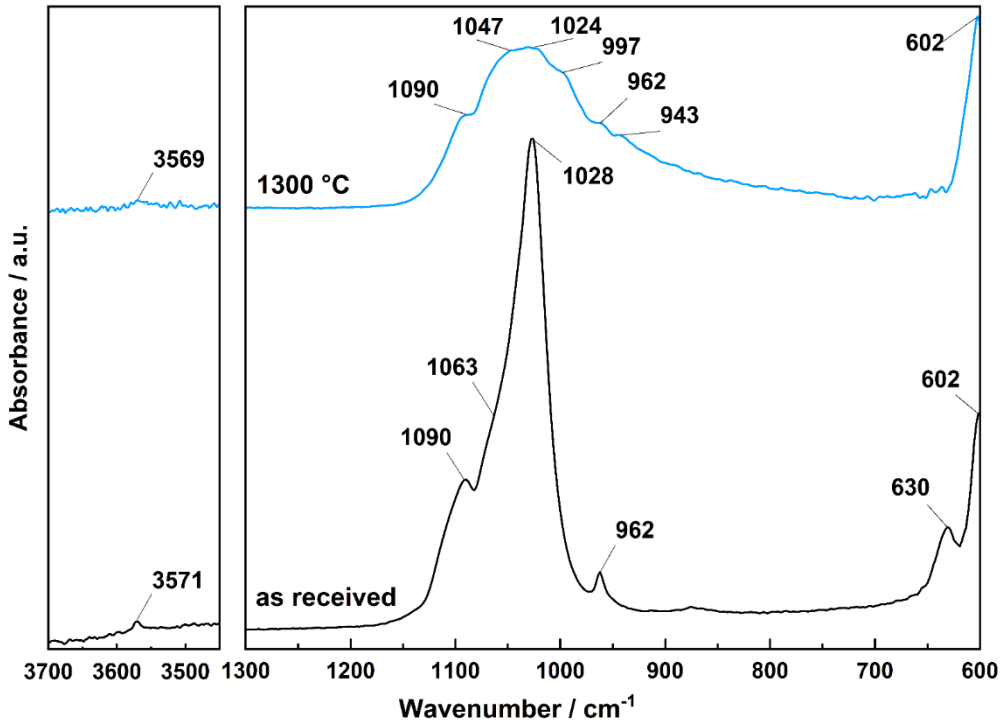

Figure 6. ATR-FTIR spectra of as received CDHA (bottom) and corresponding spectra after the material sintering at 1300 °C (top).

Surface morphology of scaffolds sintered at elevated temperatures

The morphology of the scaffolds before and after sintering observed by SEM is shown in **Figure 7**. The scaffolds printed from composite filament sintered at elevated temperatures 1200, 1300 and 1400 °C revealed linear shrinkage when compared to green body, corresponding to the values ranging from ~30-33 %.

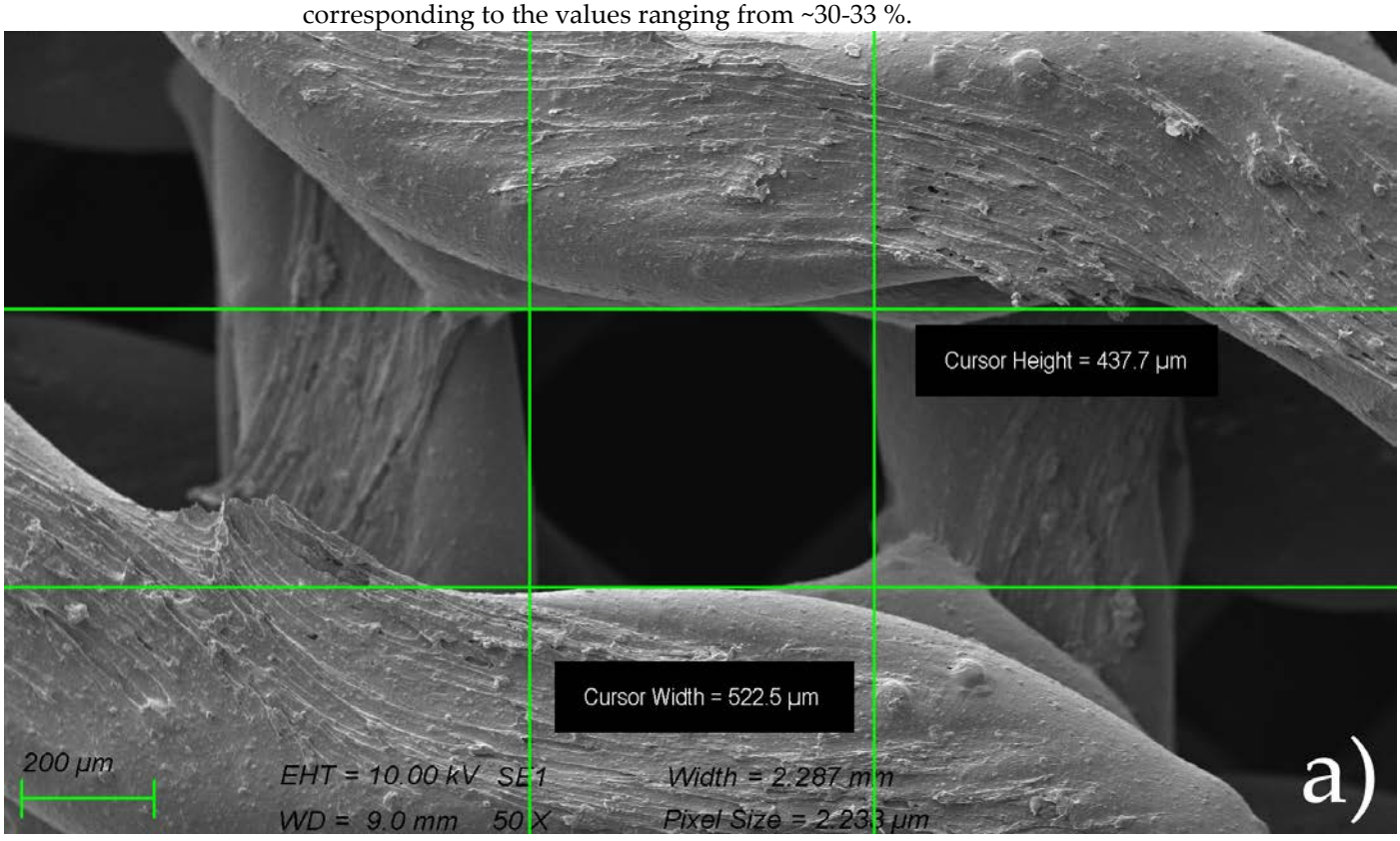

Preprints (www.preprints.org) | NOT PEER-REVIEWED | Posted: 8 November 2022 doi:10.20944/preprints202211.0141.v1

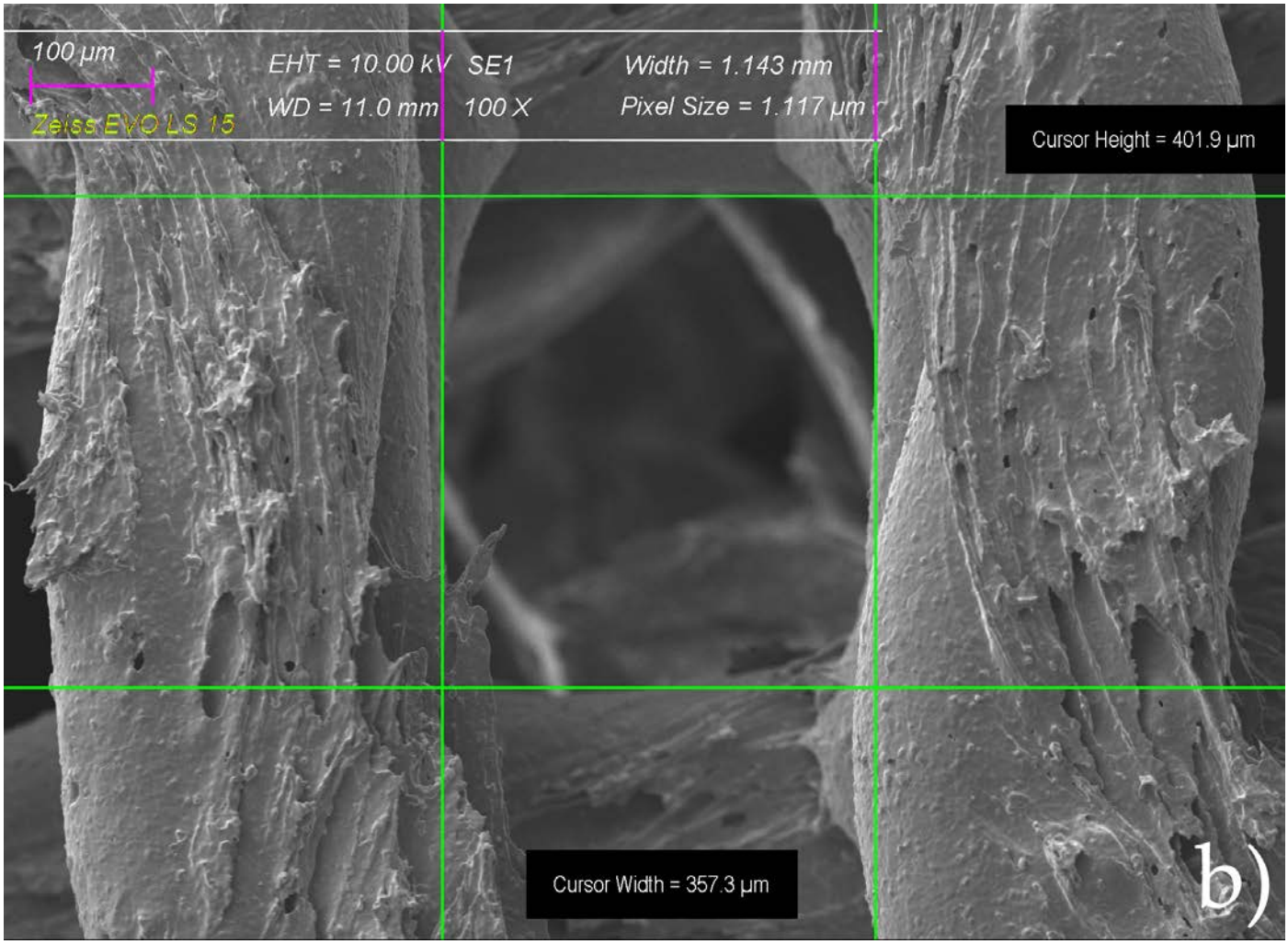

Figure 7. The morphology of the scaffolds observed by SEM before biocolonization with MSCs: (**a**) Gyroid scaffold measured before sintering; (**b**) Gyroid scaffold measured after sintering in 1400 °C.

Resulting scaffolds after biocolonization with MSC

There was no significant difference between the scaffolds sintered at elevated temperatures of 1200, 1300, and 1400 °C in terms of the architecture of the scaffold. The morphology of the MSC-populated scaffolds after sintering can be seen in Figure 8 a-c (SEM). The surface of MSCs, cultivated on the scaffold sintered at 1200 °C presented flat cells sparsely distributed over the surface of the scaffold, which was well observed by SEM. Long, elongated projections were connected to the surface and to each other (Figure 8a). Cells cultivated on a scaffold sintered at 1300 °C showed similar patterns of cell distribution, with more frequent overlapping projections (Figure 8b). And the surface of MSC culture cultivated on a scaffold sintered at 1400 °C showed a monolayer of flat cells with intense cell overlap and only a few of them with vesicles, probably due to the favorable conditions (Figure 8c).

 doi:10.20944/preprints202211.0141.v1

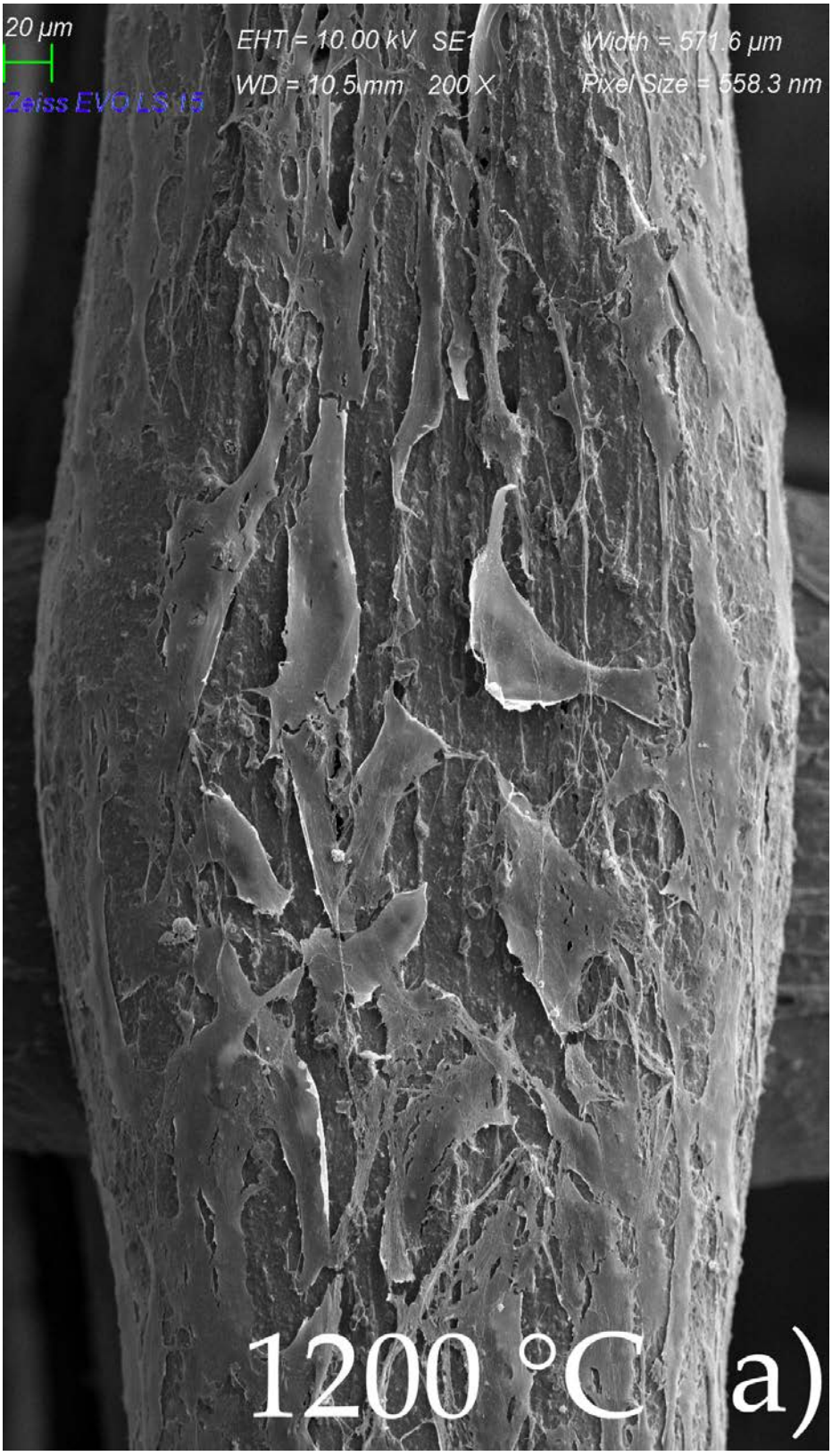

Preprints (www.preprints.org) | NOT PEER-REVIEWED | Posted: 8 November 2022 doi:10.20944/preprints202211.0141.v1

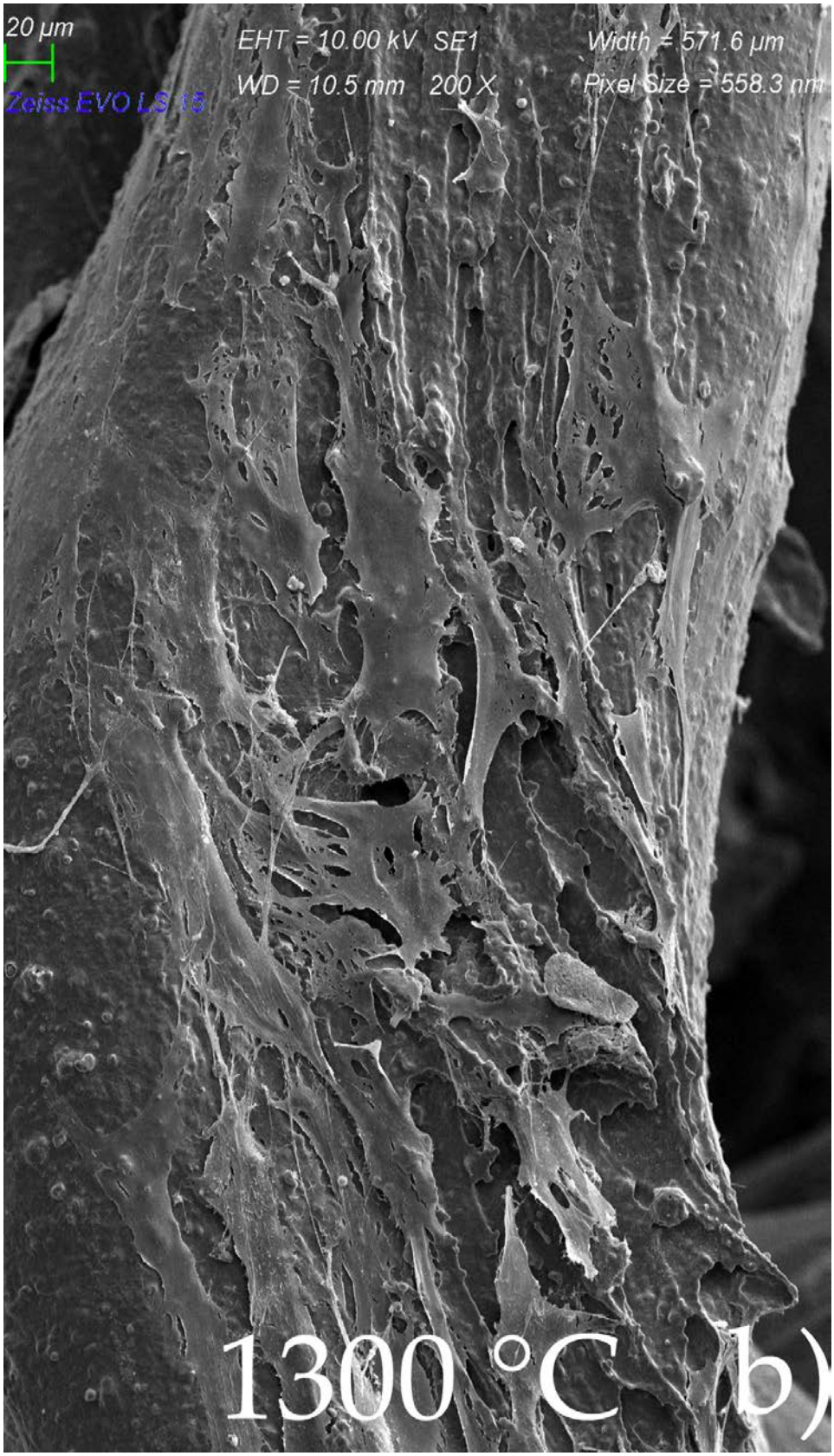

 doi:10.20944/preprints202211.0141.v1

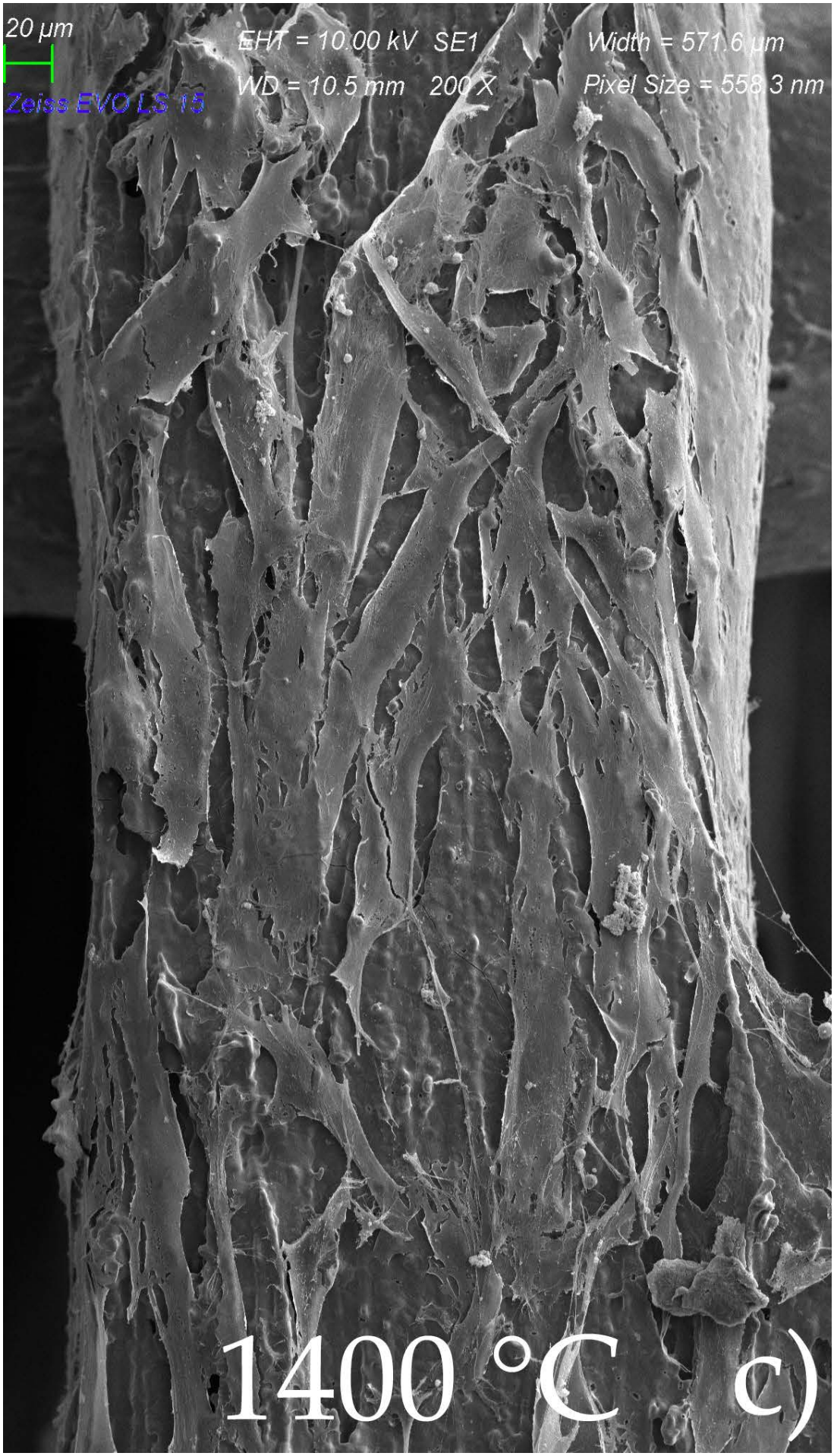

 doi:10.20944/preprints202211.0141.v1

Figure 8. Morphological SEM evaluation of biocolonization evaluated gyroid scaffolds sintered in three different temperatures (1200, 1300, and 1400 °C): (**a**) Surface of MSCs culture, cultivated on scaffold sintered at 1200 °C. SEM, Mag x200. Flat cells sparsely distributed throughout a scaffold line surface. Long elongated projections connect to the line surface and to each other; (**b**) Surface of MSCs culture, cultivated on scaffold sintered at 1300 °C. SEM, Mag x200. Similar patterns of cell distribution, projections overlap more frequently; (**c**) Surface of MSCs culture, cultivated on scaffold sintered at 1400 °C. SEM, Mag x200. Monolayer of flat cells with intensive cell overlapping and few of them with vesicles (asterisk) probably due to most beneficial conditions.

A monolayer of flat elongated or star-shaped cells covered the surface of the scaffold. Cell cultures were found on the scaffold material at the top, the bottom and even on its lateral sides. Numerous projections protruded from the cells. Long projections helped the cells to adhere to the scaffold surface and to interact with each other, as well. Several short projections overlapped the body of neighboring cell. Some cells showed smooth surface, some of them reflected an outgrowth of cell projections, with the appearance of the rough surface with vesicles. Preservation of the cell population up to the 14th day after the seeding of the cell culture was also observed with scaffolds fired at temperature 1200°C, but the population with the highest density of cells was observed for the scaffold fired at 1400°C.

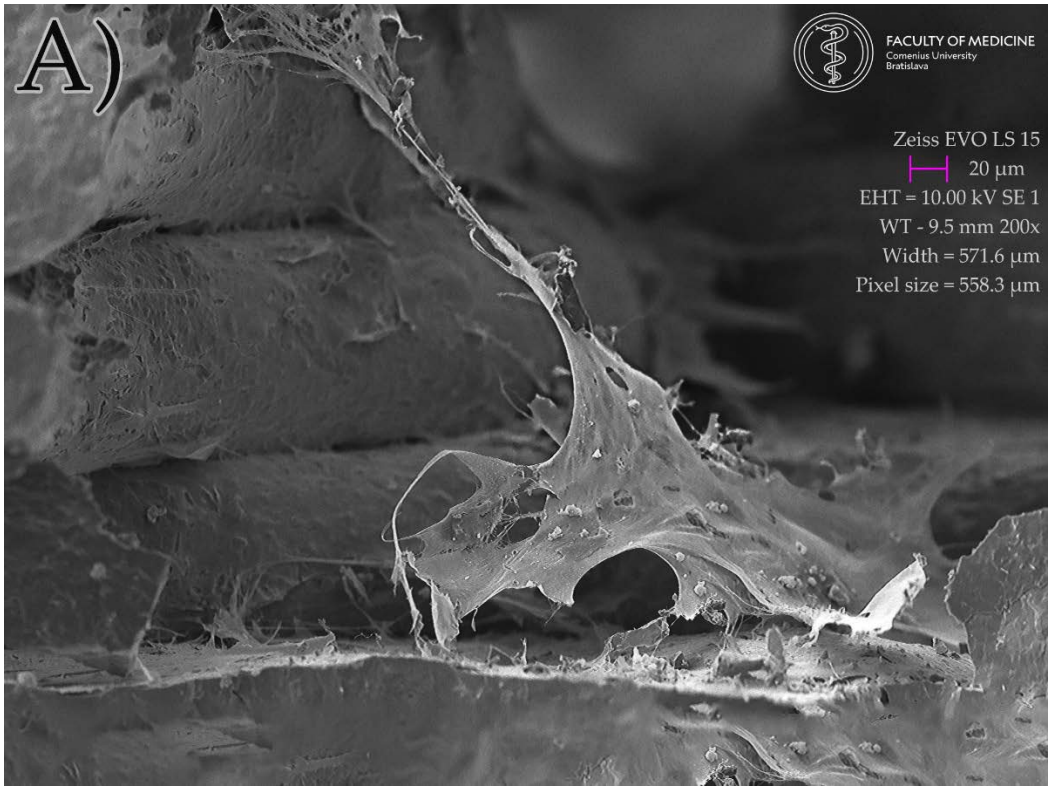

 doi:10.20944/preprints202211.0141.v1

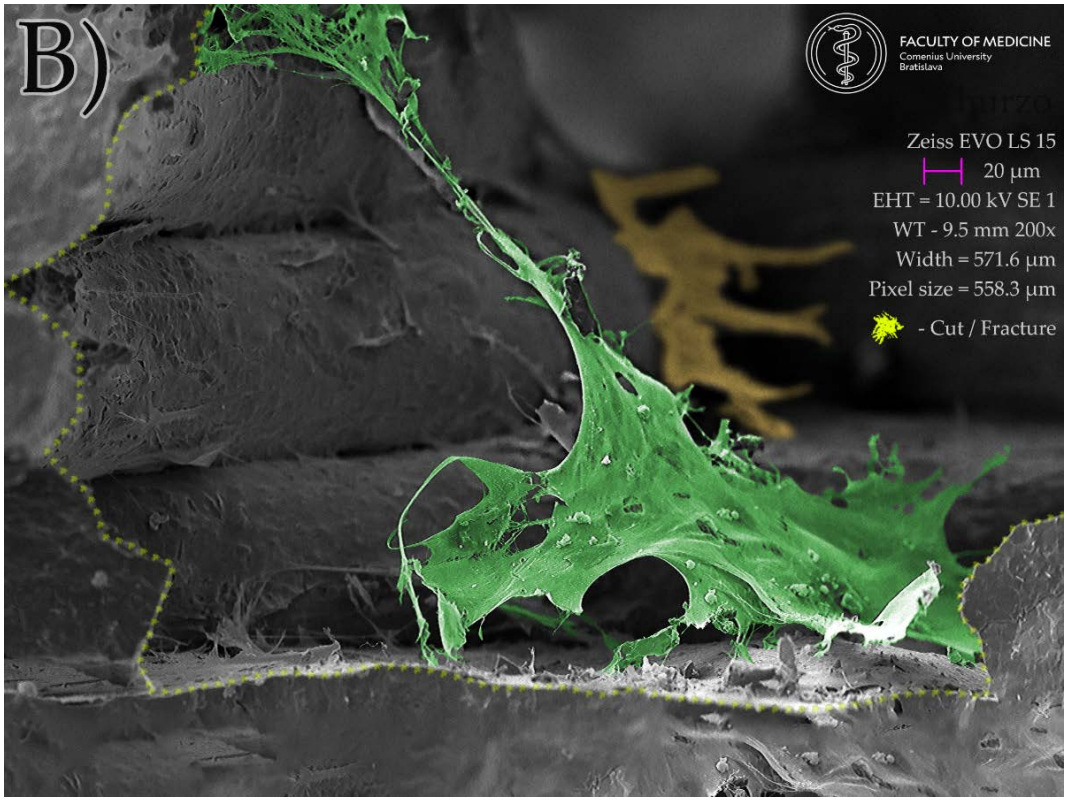

Figure 9. Lateral view of the interior of the scaffold floor, created with an ultra-sharp razor blade. Large flat cell in the foreground shows exceptionally long cell projections (arrows) firmly attached to the lateral surfaces of the scaffold. The openings between the scaffold lines appear to be a friendly environment for cell growth: (a) Original SEM image; (b) Enhanced image showing the scaffold section and the green-colored cell attached to the scaffold from bottom to the top, with a yellow-colored cell in the background climbing up in the posterior corner of the scaffold.

3. Discussion

The results of this research can be interpreted as promising signal to future perspectives of regenerative dentistry addressing needs of bone defects therapy. The findings showed that the material can be utilized in FDM manufacturing scaffolds of desired porosity with reliable geometry precision. Implications of this conclusion are important for future 3D personalization of the colonized object intended for bone defect of specific shape and size.

The findings regarding cytotoxicity of the material showed in LDH release assay and MTT assay that all analyzed materials were non-toxic which implicates suitability of this material for biocolonization and thus a possible path for desired cellular personalization.

Implications of these findings in the broadest context possible suggest feasible path in future clinical applications of this material and methods. It may also be highlighted that this paper introduces interdisciplinary cooperation of material scientists, tissue engineering experts from the fields of biology and medicine and dentists focused on regenerative dentistry. This cooperation towards utilization of this novel HA material with 3D FDM printing and MSC colonization presents a prospective setup for the repair of critical size in alveolar bone defects, which is still an unmet clinical need.

In similar research published by González-Henríquez et al. 2022, an attempt was made to create a cellular scaffold with an intricate and complex network of interconnected pores and microchannels using salt leaching and additive manufacturing (3D printing) methods that mimic the hierarchical internal structure of bone. A biocompatible hydrogel film (based on polyethylene glycol) was used to cover the top of various polymeric scaffolds. The pores had a mean size of 26.4 ± 9.9 µm, resulting in a total scaffold porosity of ~42% (including pores and microchannels) which is similar to porosity of scaffolds used

 doi:10.20944/preprints202211.0141.v1

in this study (50% porosity achieved by larger pores 350-400 μm) [41]. Limitation of scaffold thickness for clinical applications persists due to the anticipated lack vascularization in the in vivo environment.

Another recent study published in Journal of Functional Biomaterials by Mocanu et al. 2022 presented the intersection of the bone tissue reconstruction and additive manufacturing fields by introduction of a high-performance bone-like-scaffolds manufacturing. However, the strategy proposed in this paper was directed toward the use of bovine-bone-derived hydroxyapatite for surface properties enhancement and mechanical features reinforcement of the polylactic acid (PLA) matrix for composite filaments extrusion. Mocanu et al. have also used SME for analysis melt mixtures of HA+PLA and found uniform and homogenous dispersion of HA particles and an adequate adhesion at the ceramic/polymer interface, without outline pores [42].

On the contrary in our study, was utilized CDHA composed of primary HA crystals around 100 nm in size prior sintering. These were used in preparation of the composite filament with final 50 wt.% of CDHA and 50 wt.% of thermoplastic binder including polyvinyl alcohol and plasticizer [43]. The polyvinyl alcohol was used only as thermoplastic binder and was eliminated during the thermal debinding process. A possible explanation of why the material prepared at 1200°C had inhibitory effect on cell proliferation is hypothesis that some toxic remnants of the PVA produced by thermal debinding were not completely removed during sintering process, albeit this is not yet approved hypothesis.

In the clinical comparison of synthetic scaffolds and autografts in animals, a recent study by Rahyussalim et al. 2022 presented the in vivo use of 3D PLA scaffolds with HA /alginate composite injection and MSC as laminoplasty spacers in rabbits. This study investigated the in vivo biocompatibility and tissue scaffold integration of a PLA scaffold with the addition of alginate/ HA and MSC injections. This shows that the synthetic scaffolds we used had a similar tissue response and may have tissue integration profile as the autografts [44]. The results of our work encourage further scientific research and, in perspective, translational studies in animals and later in humans, so that this biocompatible scaffold can be developed to fill bone defects.

To address a final intriguing observation was the search for explanation of sudden bluish coloration of originally white scaffolds after the firing process. A possible explanation of this phenomenon is provided by previous research. As the scaffold contains traces of manganese a possible explanation of the blueish dye of the fired scaffolds is its oxidation, that occurs during the sintering process in an oxygen containing atmosphere. These phenomena have also been observed in a paleontological study searching for answers to bluish bones found. For example, results of the investigation of paleontological blue and gray bone fragments of small vertebrates coming from stratigraphic layer 770 at San Josecito Cave (Nuevo Leon, Mexico, dating between 28 000- and 19 000-years BP). Also, prior research has shown that Mn^{5+} in tetrahedral coordination could be responsible for the turquoise blue color in mastodon ivory some tens of million years old that was affected by a heat. Manganese is present in the anionic form of $(MnO_4)^{3-}$ and partially substitute for $(PO_4)^{3-}$ in the hydroxyapatite matrix. Cations of Mn^{5+} in a tetrahedral environment of four O^{2-} ions in the apatite structure are found in bluish bones at San Josecito Cave, the same color origin as in the blue mastodon ivory. The formation of Mn^{5+} is likely induced by heat treatment of the bones under oxidizing conditions [45].

 doi:10.20944/preprints202211.0141.v1

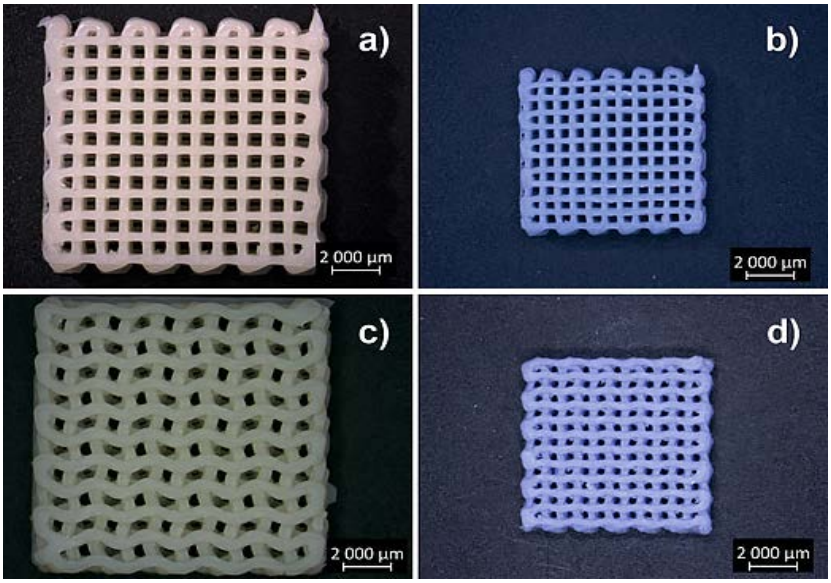

Figure 10. Optical microscopy images of 3D printed scaffolds **a)** rectilinear as printed; and **b)** sintered at 1300°C; **c)** gyroid as printed; and **d)** sintered at 1300°C.

4. Materials and Methods

Materials

Commercially available calcium deficient (CDHA) powder (Ca/P ≅ 1.54, Brenntag, Netherlands B.V.) with spherical particle aggregates having diameters ranging from ~ 1 up 200 µm with $d_{50} \leq 35$ µm determined by light scattering measurements using Malvern Instruments Ltd. Mastersizer 3000 was used. The hydroxyapatite (HA) was applied as received for preparation of composite filament from 50 wt.% of CDHA and 50 wt.% of thermoplastic polymer, polyvinylalkohol (PVA, Kuraray-POVAL™, Kuraray Europe GmbH) including plasticizer [43]. The filament with diameter 1.75 ± 0.05 mm was extruded using above mentioned pre-mixed components in double screw extruder and the desired filling grade of inorganic component after extrusion was also approved by the gravimetry after composite firing at 1300 °C to be 47.0 wt.%. The water loss in CDHA determined by thermogravimetry showed gradual water loss from room temperature (20 °C) till expected dehydroxylation temperature (800 °C) with mass change 3.78 %. This value is already above the theoretical amount of water released from stoichiometric hydroxyapatite (STHA Ca/P ≅ 1.664) reported by Markovic et al. 2004 [46]. The most of water loss in this temperature range is associated to the release of adsorbed surface water. Water formed by CDHA structure dehydroxylation resulting in formation of β-tricalcium phosphate (β-TCP) during highest temperature treatments from investigation range used (20-850 °C), reported by Markovic et al. 2004, was on the level of 6.5 % of total water amount released.

Methods

The X-ray powder diffraction (XRPD) and Fourier Transform Infrared Spectroscopy (FTIR) for better assignment of material properties and clear comparison with the past and future investigations was used. The CDHA structure changes induced by material sintering at elevated temperatures were investigated by XRPD using Brag-Bretano geometry of Stoe Thetha-Thetha goniometer equipped with linear position sensitive detector. The cobalt lamp radiation CoKα(1) with wavelength of 0.1788965 nm and measuring range of 20-70 2θ° with 0.2 step and integration time of 10 s was used. The XRPD patterns were evaluated using the software Match!© ver. 3.12 and Crystallography Open Database (COD-Inorg 2021.06.14) entrance 96-900-1234.

 doi:10.20944/preprints202211.0141.v1

The spectral features of CDHA in the mid-infrared region were revealed by infrared spectroscopy measured by ATR module PIKE MIRacle™ with ZnSe crystal using FTIR spectrometer Nicolet 6700 and DTGS detector. The spectra were measured in the range of 4000-600 cm^{-1} (due to ZnSe absorption edge at ~600 cm^{-1}) averaging 64 spectral scans with resolution of 4 cm^{-1}. The background signal was measured prior each measurement and spectra were evaluated by Omnic® (Thermo Electron Corporation) software ver. 7.1 (**Figure 6**). The water loss from HA powder was followed by thermogravimetric analysis using TG/DTA 6300 EXSTAR SII Hitachi (Japan). The scaffolds surface features and changes of microstructure of the sintered material were observed by Scanning Electron Microscopy (SEM) using a JEOL 7500 F (JEOL Ltd., Tokyo, Japan) with an accelerating voltage of 15 kV. The powder or part of scaffold was stuck on conductive tape and the surface of non-conductive ceramic was covered by gold in vacuum evaporator. The tested scaffolds were printed on a Leapfrog™ Creatr 3D printer controlled from PC by the Repetier-Host software version 2.2.2 (Hot-World GmbH & Co. KG, Germany). Scaffolds with rectilinear or by gyroid architecture of individual layers were deposited on printing platform with the size of the composite green body after printing 12.5 × 12.5 × 2.6 mm^3. A simple STL model of the test plate was created in the free available Tinkercad program, while the printing conditions and slicing were set in Repetier-Host using the slicer software Slic3r version 1.3.1. program with following parameters: Printing speed 20 $mm \cdot s^{-1}$; Filament extrusion multiplier 1.00 ×; Infill - rectangular/gyroid; Filling density - 42%, 48%, 52% / 41%, 46%, 50% (rectilinear / gyroid); Layer height - 0.2 mm; Extruder temperature - 220°C; Pad temperature - none; Nozzle diameter - 0.4 mm. The scaffolds were thermally debinded in static air atmosphere using programable oven Classic™ (Czech Republic). The debinding program was optimized according to the thermal decomposition of composite filament observed under its thermogravimetric behavior observed with heating rate of 10 $°C \cdot min^{-1}$. Hence, the slowest thermal heating rates equal to 0.1 $°C \cdot min^{-1}$ required during debinding in oven were at temperatures ~250 and ~400 °C [47]. Optical microscope images of scaffolds were collected prior and after sintering using optical microscope Zeiss Stemi 508. This was equipped with objective set enabling enlargements ranging from 0.63 to 5× and coupled with Axiocam 105 (Carl Zeiss AG, Jena, Germany).

Direct contact cytotoxicity assay

Cell proliferation and morphological changes were studied using an inverted light microscope (Zeiss Axiovert 100, Carl Zeiss, Jena, Germany).

MTT assay

The 3-(4,5-dimethylthiazol-2-yl)-2,5-diphenyltetrazolium bromide (MTT) assay (The CellTiter 96® AQueous One Solution Cell Proliferation Assay, Promega, USA) was used to analyze cell viability, for detecting the cytotoxicity and effect of material on cell growth. Sterile scaffolds were placed into a 24-well plate and rinsed with complete culture medium DMEM Low glucose supplemented with 10% FBS, 100µg/ml streptomycin, and 100U/ml penicillin (Sigma-Aldrich, USA). Afterward, adipose tissue-derived stem cells with a density of 5×10^4 cells per well were seeded on the scaffolds, followed by incubating at 37 °C for 48 h. At the end of the incubation, 10µl of MTT solution was added, followed by 4 h incubation. The supernatant was aspired and transferred into a new plate and absorbance was recorded at 490 nm using a plate reader BioTek EL800 (BioTek, USA). All experiments were performed in triplicate.

LDH Release Assay

Cytotoxicity induced by scaffolds was evaluated by lactate dehydrogenase (LDH) release assay (Sigma-Aldrich). LDH assay mixture was prepared by mixing equal volumes of LDH assay substrate solution, LDH assay dye solution, and 1x LDH assay co-

 doi:10.20944/preprints202211.0141.v1

factor preparation. An aliquot of the medium was aspirated, and Lactate Dehydrogenase Assay mixture was added to each sample. The plate was covered with an opaque material to protect against light and incubated at room temperature for 20 – 30 minutes. Absorbance was measured spectrophotometrically at the wavelength of 490 and 630 nm using a plate reader BioTek EL 800. All experiments were performed in triplicate.

Methods of sample preparation for scanning electron microscopy:

The cell cultures adhered on scaffolds in culture medium were gently washed by 3% glutaraldehyde buffered solution fixative for 30 minutes at room temperature. Afterwards, samples were rinsed three times in phosphate buffer solution and postfixed in osmium tetroxide solution for 1 hour at 4°C temperature. After the rinse in demineralized water, samples were dehydrated through a graded ethanol series to 100% ethanol, followed by critical point drying of liquid CO_2 . Finally, they were mounted on aluminum specimen stubs with carbon adhesive tapes, sputter coated with 7 nm layer of gold/palladium and examined with a scanning electron microscope ZEISS type EVO LS 15.

Statistical analysis

All quantitative results were obtained from at least triplicate samples. Data are expressed as the mean ± standard deviation. Statistical analysis between groups was conducted using single-factor analysis of variance (ANOVA). A value of $P<0.05$ was considered to be statistically significant.

5. Conclusions

This proof-of-concept study presents a feasible fabrication of CDHA/PVA composite filament, FDM 3D printing of CDHA scaffold, heat postprocessing and sintering of the scaffold was followed by colonization with MSC. In vitro characterization of the material with MTT and LDH assays has proven the resulting CDHA based scaffold as non-toxic and biocompatible with good cellular adherence evaluated morphologically by SEM.

Gyroid or rectilinear geometrical organization of the pores had no significant impact on cell colonization and adherence, however, higher temperatures of scaffold sintering was more suitable for cell colonization. Scaffold fired at the lowest temperature of 1200 °C showed even inhibitory effect on cell proliferation.

In conclusion, based on all results obtained, it can be emphasized that novel hydroxyapatite scaffolds produced by 3D printing have great potential to be used in the tissue engineering of bones. However, further in vitro and in vivo studies on their osteoinductive potential and biosafety need to be conducted to support translation into clinical applications.

Author Contributions: Conceptualization, A.T.; Ľ.D.; I.V.; J.F. and M.J.; methodology, A.T.; Ľ.D. and M.J.; software, A.T.; P.G.; Ľ.D. and M.J.; validation, A.T.; Ľ.D.; I.V.; J.F.. and M.J.; formal analysis, A.T.; Ľ.D.; I.V.; J.F.; P.G.; Z.V.N.; Š.P.; I.V.; M.S.; R.U.; J.S. and M.J.; investigation, A.T.; P.G.; Ľ.D.; M.J.; Ľ.L.; resources, Z.H.; J.F.; M.J. and Ľ.D.; data curation, A.T.; writing—original draft preparation, A.T.; writing—review and editing, A.T.;P.G.; Z.V.N.;Š.P.;I.V.; M.S.;R.U.;J.S.; Ľ.L.; Z.H.; J.F.;M.J.; Ľ.D.; visualization, A.T.; P.G.; M.J.; +L.D. and Z.V.N.; supervision, Ľ.D.; Project administration, M.J.; funding acquisition, Ľ.D. and M.J. All authors have read and agreed to the published version of the manuscript.

Funding: This work was supported by the Slovak Grant Agency for Science VEGA grant No. 1/0342/21 and Slovak Research and Development Agency under Contracts no. APVV-21-0173 and APVV-16-0341. This work was also created thanks to the support of the Operational Program Integrated infrastructure for the project: Advancing University Capacity and Competence in Research,

Development and Innovation ("ACCORD") ITMS2014 +: 313021X329, co-financed by resources of the European Regional Development Fund.

Institutional Review Board Statement: The study was conducted in accordance with the Declaration of Helsinki. Ethical review and approval were waived for this study as it was not conducted on humans or animals.

Data Availability Statement: Not applicable.

Acknowledgments: The authors gratefully acknowledge the technological support of the digital dental lab infrastructure of 3Dent Medical Ltd. company as well as dental clinic Sangre Azul Ltd.

Conflicts of Interest: The authors declare no conflict of interest.

References

1. Barrows, T. Degradable Implant Materials: A Review of Synthetic Absorbable Polymers and Their Applications. *Clin Mater* **1986**, *1*, 233–257, doi:10.1016/S0267-6605(86)80015-4.
2. Palmer, L.C.; Newcomb, C.J.; Kaltz, S.R.; Spoerke, E.D.; Stupp, S.I. Biomimetic Systems for Hydroxyapatite Mineralization Inspired by Bone and Enamel. *Chem Rev* **2008**, *108*, 4754–4783, doi:10.1021/CR8004422.
3. Gallo, S.; Pascadopoli, M.; Pellegrini, M.; Pulicari, F.; Manfredini, M.; Zampetti, P.; Spadari, F.; Maiorana, C.; Scribante, A. Latest Findings of the Regenerative Materials Application in Periodontal and Peri-Implant Surgery: A Scoping Review. *Bioengineering 2022, Vol. 9, Page 594* **2022**, *9*, 594, doi:10.3390/BIOENGINEERING9100594.
4. Devlin, H.; Ferguson, M.W. Alveolar Ridge Resorption and Mandibular Atrophy. A Review of the Role of Local and Systemic Factors. *British Dental Journal 1991 170:3* **1991**, *170*, 101–104, doi:10.1038/sj.bdj.4807427.
5. Hansson, S.; Halldin, A. Alveolar Ridge Resorption after Tooth Extraction: A Consequence of a Fundamental Principle of Bone Physiology. *J Dent Biomech* **2012**, *3*, 1–8, doi:10.1177/1758736012456543.
6. Hou, X.; Zhang, L.; Zhou, Z.; Luo, X.; Wang, T.; Zhao, X.; Lu, B.; Chen, F.; Zheng, L. Calcium Phosphate-Based Biomaterials for Bone Repair. *Journal of Functional Biomaterials 2022, Vol. 13, Page 187* **2022**, *13*, 187, doi:10.3390/JFB13040187.
7. Zhao, D.W.; Fan, X.C.; Zhao, Y.X.; Zhao, W.; Zhang, Y.Q.; Zhang, R.H.; Cheng, L. Biocompatible Nano-Hydroxyapatites Regulate Macrophage Polarization. *Materials 2022, Vol. 15, Page 6986* **2022**, *15*, 6986, doi:10.3390/MA15196986.
8. Azmah Hanim, M.A.; Calin, R.; Jung, D.W. PLA-Based Bionanocomposites in Tissue Engineering and Regenerative Medicine. *Bionanocomposites in Tissue Engineering and Regenerative Medicine* **2021**, 481–497, doi:10.1016/B978-0-12-821280-6.00002-7.
9. Ielo, I.; Calabrese, G.; de Luca, G.; Conoci, S. Recent Advances in Hydroxyapatite-Based Biocomposites for Bone Tissue Regeneration in Orthopedics. *International Journal of Molecular Sciences 2022, Vol. 23, Page 9721* **2022**, *23*, 9721, doi:10.3390/IJMS23179721.
10. Pupilli, F.; Ruffini, A.; Dapporto, M.; Tavoni, M.; Tampieri, A.; Sprio, S. Design Strategies and Biomimetic Approaches for Calcium Phosphate Scaffolds in Bone Tissue Regeneration. *Biomimetics 2022, Vol. 7, Page 112* **2022**, *7*, 112, doi:10.3390/BIOMIMETICS7030112.
11. Kim, Y.; Lee, E.J.; Kotula, A.P.; Takagi, S.; Chow, L.; Alimperti, S. Engineering 3D Printed Scaffolds with Tunable Hydroxyapatite. *Journal of Functional Biomaterials 2022, Vol. 13, Page 34* **2022**, *13*, 34, doi:10.3390/JFB13020034.
12. Kim, Y.; Lee, E.J.; Davydov, A. v.; Frukhtbeyen, S.; Seppala, J.E.; Takagi, S.; Chow, L.; Alimperti, S. Biofabrication of 3D Printed Hydroxyapatite Composite Scaffolds for Bone Regeneration. *Biomedical Materials* **2021**, *16*, 045002, doi:10.1088/1748-605X/ABCF03.

13. Thurzo, A.; Urbanová, W.; Neuschlová, I.; Paouris, D.; Čverha, M. Use of Optical Scanning and 3D Printing to Fabricate Customized Appliances for Patients with Craniofacial Disorders. *Semin Orthod* **2022**, *0*, 1–11, doi:10.1053/j.sodo.2022.10.005.
14. Thurzo, A.; Šufliarsky, B.; Urbanová, W.; Čverha, M.; Strunga, M.; Varga, I. Pierre Robin Sequence and 3D Printed Personalized Composite Appliances in Interdisciplinary Approach. *Polymers (Basel)* **2022**, *14*, 3858, doi:10.3390/polym14183858.
15. Thurzo, A.; Urbanová, W.; Novák, B.; Waczulíková, I.; Varga, I. Utilization of a 3D Printed Orthodontic Distalizer for Tooth-Borne Hybrid Treatment in Class II Unilateral Malocclusions. *Materials* **2022**, *15*, 1740, doi:10.3390/ma15051740.
16. Thurzo, A.; Kočiš, F.; Novák, B.; Czako, L.; Varga, I. Three-Dimensional Modeling and 3D Printing of Biocompatible Orthodontic Power-Arm Design with Clinical Application. *Applied Sciences* **2021**, *11*, 9693, doi:10.3390/app11209693.
17. Csöbönyeiová, M.; Beerová, N.; Klein, M.; Debreová-ˇ Ceháková, M.; Uboš Danišovič, L.' Cell-Based and Selected Cell-Free Therapies for Myocardial Infarction: How Do They Compare to the Current Treatment Options? *International Journal of Molecular Sciences 2022, Vol. 23, Page 10314* **2022**, *23*, 10314, doi:10.3390/IJMS231810314.
18. Osouli-Bostanabad, K.; Masalehdan, T.; Kapsa, R.M.I.; Quigley, A.; Lalatsa, A.; Bruggeman, K.F.; Franks, S.J.; Williams, R.J.; Nisbet, D.R. Traction of 3D and 4D Printing in the Healthcare Industry: From Drug Delivery and Analysis to Regenerative Medicine. *ACS Biomater Sci Eng* **2022**, doi:10.1021/ACSBIOMATERIALS.2C00094/ASSET/IMAGES/MEDIUM/AB2C00094_0010.GIF.
19. Zhang, Y.; Yu, Y.; Akkouch, A.; Dababneh, A.; Dolati, F.; Ozbolat, I.T. In Vitro Study of Directly Bioprinted Perfusable Vasculature Conduits. *Biomater Sci* **2014**, *3*, 134–143, doi:10.1039/C4BM00234B.
20. Bose, S.; Vahabzadeh, S.; Bandyopadhyay, A. Bone Tissue Engineering Using 3D Printing. *Materials Today* **2013**, *16*, 496–504, doi:10.1016/J.MATTOD.2013.11.017.
21. Genova, T.; Roato, I.; Carossa, M.; Motta, C.; Cavagnetto, D.; Mussano, F. Advances on Bone Substitutes through 3D Bioprinting. *International Journal of Molecular Sciences 2020, Vol. 21, Page 7012* **2020**, *21*, 7012, doi:10.3390/IJMS21197012.
22. Quigley, A.F.; Razal, J.M.; Thompson, B.C.; Moulton, S.E.; Kita, M.; Kennedy, E.L.; Clark, G.M.; Wallace, G.G.; Kapsa, R.M.I. A Conducting-Polymer Platform with Biodegradable Fibers for Stimulation and Guidance of Axonal Growth. *Advanced Materials* **2009**, *21*, 4393–4397, doi:10.1002/adma.200901165.
23. Wiatrak, B.; Sobierajska, P.; Szandruk-Bender, M.; Jawien, P.; Janeczek, M.; Dobrzynski, M.; Pistor, P.; Szelag, A.; Wiglusz, R.J. *Bionanocomposites in Tissue Engineering and Regenerative Medicine*; Elsevier, 2021; Vol. 22; ISBN 9780128212806.
24. Miranda, C.C.; Gomes, M.R.; Moço, M.; Cabral, J.M.S.; Ferreira, F.C.; Sanjuan-Alberte, P.A.; Zarrabi, A.; Miranda, C.C.; Gomes, M.R.; Moço, M.; et al. A Concise Review on Electrospun Scaffolds for Kidney Tissue Engineering. *Bioengineering 2022, Vol. 9, Page 554* **2022**, *9*, 554, doi:10.3390/BIOENGINEERING9100554.
25. Stocco, E.; Barbon, S.; Zeni, E.; Cassari, L.; Zamuner, A.; Gloria, A.; Russo, T.; Boscolo-Berto, R.; Sfriso, M.M.; Macchi, V.; et al. Development of Two-Layer Hybrid Scaffolds Based on Oxidized Polyvinyl Alcohol and Bioactivated Chitosan Sponges for Tissue Engineering Purposes. *International Journal of Molecular Sciences 2022, Vol. 23, Page 12059* **2022**, *23*, 12059, doi:10.3390/IJMS232012059.
26. Feng, Y.; Dai, S.-C.; Lim, K.; Ramaswamy, Y.; Jabbarzadeh, A.; Tribological, R.; M˘arginean, M.; Cojocaru, V.; Frunzăverde, D.; Mele, A.; et al. Tribological and Rheological Properties of Poly(Vinyl Alcohol)-Gellan Gum Composite Hydrogels. *Polymers 2022, Vol. 14, Page 3830* **2022**, *14*, 3830, doi:10.3390/POLYM14183830.

27. Seredin, P.; Goloshchapov, D.; Kashkarov, V.; Khydyakov, Y.; Nesterov, D.; Ippolitov, I.; Ippolitov, Y.; Vongsvivut, J. Development of a Hybrid Biomimetic Enamel-Biocomposite Interface and a Study of Its Molecular Features Using Synchrotron Submicron ATR-FTIR Microspectroscopy and Multivariate Analysis Techniques. *International Journal of Molecular Sciences 2022, Vol. 23, Page 11699* **2022**, *23*, 11699, doi:10.3390/IJMS231911699.
28. Cestari, F.; Yang, Y.; Wilbig, J.; Günster, J.; Motta, A.; Sglavo, V.M. Powder 3D Printing of Bone Scaffolds with Uniform and Gradient Pore Sizes Using Cuttlebone-Derived Calcium Phosphate and Glass-Ceramic. *Materials 2022, Vol. 15, Page 5139* **2022**, *15*, 5139, doi:10.3390/MA15155139.
29. Devi G.V., Y.; Nagendra, A.H.; Shenoy P., S.; Chatterjee, K.; Venkatesan, J. Fucoidan-Incorporated Composite Scaffold Stimulates Osteogenic Differentiation of Mesenchymal Stem Cells for Bone Tissue Engineering. *Mar Drugs* **2022**, *20*, 589, doi:10.3390/md20100589.
30. Baru, O.; Nutu, A.; Braicu, C.; Cismaru, C.A.; Berindan-Neagoe, I.; Buduru, S.; Badea, M. Angiogenesis in Regenerative Dentistry: Are We Far Enough for Therapy? *International Journal of Molecular Sciences 2021, Vol. 22, Page 929* **2021**, *22*, 929, doi:10.3390/IJMS22020929.
31. Tüzün-Antepli, B.; Şeker, Ş.; Elçin, A.E.; Khang, G.; Elçin, Y.M. Evaluation of Human Osteoblasts on NIPS Micro-Patterned PCL Carriers Containing Nanohydroxyapatite and Reduced Graphene Oxide Using PSμM. *Molecules* **2022**, *27*, 7091, doi:10.3390/molecules27207091.
32. Limraksasin, P.; Kondo, T.; Zhang, M.; Okawa, H.; Osathanon, T.; Pavasant, P.; Egusa, H. In Vitro Fabrication of Hybrid Bone/Cartilage Complex Using Mouse Induced Pluripotent Stem Cells. *International Journal of Molecular Sciences 2020, Vol. 21, Page 581* **2020**, *21*, 581, doi:10.3390/IJMS21020581.
33. Smojver, I.; Katalinić, I.; Bjelica, R.; Gabrić, D.; Matišić, V.; Molnar, V.; Primorac, D. Mesenchymal Stem Cells Based Treatment in Dental Medicine: A Narrative Review. *International Journal of Molecular Sciences 2022, Vol. 23, Page 1662* **2022**, *23*, 1662, doi:10.3390/IJMS23031662.
34. Tatullo, M.; Codispoti, B.; Paduano, F.; Nuzzolese, M.; Makeeva, I. Strategic Tools in Regenerative and Translational Dentistry. *International Journal of Molecular Sciences 2019, Vol. 20, Page 1879* **2019**, *20*, 1879, doi:10.3390/IJMS20081879.
35. Fonticoli, L.; della Rocca, Y.; Rajan, T.S.; Murmura, G.; Trubiani, O.; Oliva, S.; Pizzicannella, J.; Marconi, G.D.; Diomede, F. A Narrative Review: Gingival Stem Cells as a Limitless Reservoir for Regenerative Medicine. *International Journal of Molecular Sciences 2022, Vol. 23, Page 4135* **2022**, *23*, 4135, doi:10.3390/IJMS23084135.
36. Rusu, L.-C.; Ardelean, L.C.; Mohd, N.; Razali, M.; Ghazali, M.J.; Hayaty, N.; Kasim, A. Current Advances of Three-Dimensional Bioprinting Application in Dentistry: A Scoping Review. *Materials 2022, Vol. 15, Page 6398* **2022**, *15*, 6398, doi:10.3390/MA15186398.
37. Gugliandolo, A.; Fonticoli, L.; Trubiani, O.; Rajan, T.S.; Marconi, G.D.; Bramanti, P.; Mazzon, E.; Pizzicannella, J.; Diomede, F. Oral Bone Tissue Regeneration: Mesenchymal Stem Cells, Secretome, and Biomaterials. *International Journal of Molecular Sciences 2021, Vol. 22, Page 5236* **2021**, *22*, 5236, doi:10.3390/IJMS22105236.
38. Ebrahimi, M.; Botelho, M. Biphasic Calcium Phosphates (BCP) of Hydroxyapatite (HA) and Tricalcium Phosphate (TCP) as Bone Substitutes: Importance of Physicochemical Characterizations in Biomaterials Studies. *Data Brief* **2017**, *10*, 93–97, doi:10.1016/J.DIB.2016.11.080.
39. Denry, I.; Kuhn, L.T. Design and Characterization of Calcium Phosphate Ceramic Scaffolds for Bone Tissue Engineering. *Dental Materials* **2016**, *32*, 43–53, doi:10.1016/J.DENTAL.2015.09.008.
40. Fowler, B.O. Infrared Studies of Apatites. I. Vibrational Assignments for Calcium, Strontium, and Barium Hydroxyapatites Utilizing Isotopic Substitution. *Inorg Chem* **1974**, *13*, 194–207, doi:10.1021/IC50131A039/ASSET/IC50131A039.FP.PNG_V03.

41. González-Henríquez, C.M.; Rodríguez-Umanzor, F.E.; Acuña-Ruiz, N.F.; Vera-Rojas, G.E.; Terraza-Inostroza, C.; Cohn-Inostroza, N.A.; Utrera, A.; Sarabia-Vallejos, M.A.; Rodríguez-Hernández, J. Fabrication and Testing of Multi-Hierarchical Porous Scaffolds Designed for Bone Regeneration via Additive Manufacturing Processes. *Polymers 2022, Vol. 14, Page 4041* **2022**, *14*, 4041, doi:10.3390/POLYM14194041.
42. Mocanu, A.-C.; Miculescu, F.; Dascălu, C.-A.; Voicu, Ștefan I.; Pandele, M.-A.; Ciocoiu, R.-C.; Batalu, D.; Dondea, S.; Mitran, V.; Ciocan, L.-T. Influence of Ceramic Particles Size and Ratio on Surface—Volume Features of the Naturally Derived HA-Reinforced Filaments for Biomedical Applications. *Journal of Functional Biomaterials 2022, Vol. 13, Page 199* **2022**, *13*, 199, doi:10.3390/JFB13040199.
43. Janek, M.; Žilinská, V.; Kovár, V.; Hajdúchová, Z.; Tomanová, K.; Peciar, P.; Veteška, P.; Gabošová, T.; Fialka, R.; Feranc, J.; et al. Mechanical Testing of Hydroxyapatite Filaments for Tissue Scaffolds Preparation by Fused Deposition of Ceramics. *J Eur Ceram Soc* **2020**, *40*, 4932–4938, doi:10.1016/J.JEURCERAMSOC.2020.01.061.
44. Rahyussalim, A.J.; Aprilya, D.; Handidwiono, R.; Whulanza, Y.; Ramahdita, G.; Kurniawati, T. The Use of 3D Polylactic Acid Scaffolds with Hydroxyapatite/Alginate Composite Injection and Mesenchymal Stem Cells as Laminoplasty Spacers in Rabbits. *Polymers 2022, Vol. 14, Page 3292* **2022**, *14*, 3292, doi:10.3390/POLYM14163292.
45. Chadefaux, C.; Vignaud, C.; Chalmin, E.; Robles-Camacho, J.; Arroyo-Cabrales, J.; Johnson, E.; Reiche, I. Color Origin and Heat Evidence of Paleontological Bones: Case Study of Blue and Gray Bones from San Josecito Cave, Mexico. *American Mineralogist* **2009**, *94*, 27–33, doi:10.2138/am.2009.2860.
46. Markovic, M.; Fowler, B.O.; Tung, M.S. Preparation and Comprehensive Characterization of a Calcium Hydroxyapatite Reference Material. *J Res Natl Inst Stand Technol* **2004**, *109*, 553, doi:10.6028/JRES.109.042.
47. Veteška, P.; Hajdúchová, Z.; Feranc, J.; Tomanová, K.; Milde, J.; Kritikos, M.; Bača, Ľ.; Janek, M. Novel Composite Filament Usable in Low-Cost 3D Printers for Fabrication of Complex Ceramic Shapes. *Appl Mater Today* **2021**, *22*, 100949, doi:10.1016/J.APMT.2021.100949.